Available online at www.sciencedirect.com

ScienceDirect

Procedia CIRP 117 (2023) 110–115

www.elsevier.com/locate/procedia

19th CIRP Conference on Modeling of Machining Operations

Finite Element Simulation of the process combination Hammering Turning

Jannik Schwalm[a,*], Felix Mann[b], Germán González[a], Frederik Zanger[a], Volker Schulze[a]

[a]wbk Institute of Production Science, Karlsruhe Institute of Technology (KIT), Kaiserstr. 12, 76131 Karlsruhe, Germany
[b]Faculty of Mechanical Engineering, Karlsruhe Institute of Technology (KIT), Kaiserstr. 12, 76131 Karlsruhe, Germany

* Corresponding author. Tel.: +49-721-608-42455; fax: +49-721-608-45005. E-mail address: jannik.schwalm@kit.edu

Abstract

In the process combination of Hammering Turning, the workpiece surface is microtextured during machining by means of a multi-axis superimposed oscillation of the cutting tool. These microtextures are formed by plastic deformation of the surface layer in a process phase without material removal. In this paper, the formation of the microtexture in the originally three-dimensional process is investigated in simplified analogue 2D FEM simulations. This therefore only represents the processes and mechanisms directly below the cutting edge. The influence of the tool orientation on the plastic material flow and the formation of the microtexture as well as the residual stresses in the surface layer is investigated.

Keywords: surface texturing; mechanical surface treatment; piezoelectric tool system

1. Introduction

The functionalisation of surfaces for tribological applications can be achieved by means of microtexturing. The geometric shape of these textures can range from simple dimples to complex structures and has already been widely investigated [1]. Although these microtextures are used for technical applications, they often come from the field of bionics or are inspired by it. These microtextures modify the tribological properties of the contact system leading for instance to a drag reduction (shark skin) or to increase the wear resistance (beetle body), as well as to reduce the adhesion (surface of the lotus flower) or to increase it (Gecko feet) [2]. The manufacturing of these microtextures can be divided into four main groups according to their physical principle. These are the addition as well as the removal of material on a surface. Examples of this are chemical or galvanic texturing, by depositing or etching a masked surface. Similar to this is the self-forming by inhomogeneous wear resistance of a surface. The locally concentrated removal through wear of the surface leads to texturing. These methods of microtexturing, targeted material deposition or removal and self-forming through wear lead to a change in volume. The fourth method of texturing a surface is material displacement at constant volume. Here, the geometric modification of the surface takes place through plastic deformation and redistribution of material [1].

Vibration-Assisted Machining (VAM) is an option for mechanical microtexturing that was first introduced in the late 1950s. In this process, the tool or workpiece is excited with high-frequency vibrations of small amplitude in order to improve the cutting performance or to create a texture during machining. The tools for VAM can be divided into two groups, the resonant and non-resonant oscillators. The distinction is based on the type and frequency of the vibration. Resonant oscillators always work with a natural frequency and are therefore designed for one operating point. Non-resonant systems have a higher flexibility, but this is at the expense of the maximum achievable frequencies. Both systems can be excited electromagnetically or piezoelectrically [3]. Greco et al. have described a non-resonant system for the microtexturing of surfaces where a vibration in the radial direction is superimposed on the machining during turning. For this

10.1016/j.procir.2023.03.020

purpose, a single-axis piezoelectrically actuated tool system was developed, which vibrates non-resonantly at up to 200 Hz. With this system, surfaces with dimples pattern were generated. The formation of this microtexture is achieved by machining and removal of material and not by plastic deformation [4]. A resonant oscillating system was also presented by Liu et al. This system works in the ultrasonic range up to *20 kHz*, but with a small amplitude of *3.9 µm*. In geometric simulations of the surface and experimentally, it can be shown that through the selection of the process parameters, anisotropic scale-like microtextures can be generated by a flank collision of the tool with the surface [5]. In tribological investigations it could be shown that the coefficient of friction is reduced by up to 33% and that there is an increased wear resistance in the lubricated friction contact. However, due to the simultaneous machining and microtexturing, only a slight plastic deformation of the surface layer could be observed [6]. In these systems, however, the microtexture is formed during machining, with minimal plastic deformation of the surface layer and no dominant hardening. The innovative combined Hammering Turning is an approach that, in contrast to VAM, follows a synchronised kinematic approach. The aim is to achieve a hardening and increase of the residual compressive stresses as well as a microtextured surface. In this research work, the advantages of Hammering Turning compared to VAM with regard to the resulting residual stresses are to be investigated. Here, the focus is particularly on the range of material changes and residual stresses. Simplified 2D FEM simulations of the actual three-dimensional process are carried out, which allow a qualitative analysis of the surface layer states.

2. Material and Method

2.1. Process description Hammering Turning

Hammering Turning represents a novel process combination of Vibration Assisted Machining (VAM), which combines machining with mechanical surface treatment and microtexturing. A synchronized biaxial vibration and hammer stroke of the tool, which is superimposed on the cutting process, enables microtexturing by plastic deformation of the surface with the help of the cutting edge. The novelty of the process is that due to the sinusoidal oscillation of the tool in the cutting direction, the normally continuous chip formation during turning is periodically interrupted in a singular manner, so that there is no relative movement between the tool and the rotating workpiece. The kinematic boundary conditions for Hammering Turning are described in detail in Schwalm et al. [7]. By this decoupling of the chip formation, the plastic microtexturing of the surface can take place without a disturbing tangential relative movement and a maximum of plastic deformation can be obtained.

2.2. Simulation Setup

For the simulative investigation of Hammering Turning, the three-dimensional process was simplified and modeled as a two-dimensional process. This enables a qualitative investigation of the parameters influencing the residual stresses as well as the analysis of the material flow. The process parameters used for the simulation are listed in Table 1. The computation was performed with the finite element solver MSC-Marc®. The evaluation of the stresses was done on a formed texture element or tool indentation directly after processing by the tool. This local texture element is formed by a tool indentation and the first following hammer stroke and is referred to as the 1. stroke. The evaluation of the parameters remains fixed at this point in the further process in order to be able to recognise changes due to further processing. Four further hammer strokes are considered up to the 5th stroke, referred to as the 5. Stroke, this is shown in Figure 1. Since the material has not yet been cooled and the stresses introduced by the tool in contact are also effective, these are not residual stresses in the true sense of the word. To determine the residual stresses in the surface layer, the tool was removed in the simulation and a cooling time of *30 s* was applied. This is sufficient to cool the component down to an almost environmental temperature of *20°C*. In the digrams, the term used is "aftercooling". In the simulations, Hammering Turning with its biaxial movement is considered. In addition, this new process is compared with the one-dimensional VAM, which has a uniaxial hammering movement superimposed to turning. This itself represents a partial process of Hammering Turning, in which, however, no decoupling of the cutting takes place by means of the superimposed oscillation. Thus, this process exhibits a tangential sliding velocity during the hammering movement. This process is referred to in the diagrams as “VAM”. In addition to these two processes with superimposed kinematics, conventional turning is considered. A schematic sketch is given in Figure 2.

Table 1: Process parameters

Process parameters	Value
Cutting speed v_c [m/min]	3.5
Related main frequency $f_{c,o}$ [Hz]	928
Cutting depth a_p [mm]	0.1
Amplitude oscillation $A_{c,o}$ [µm] (sinusoidal)	10
Stroke hammering A_h [µm]	20

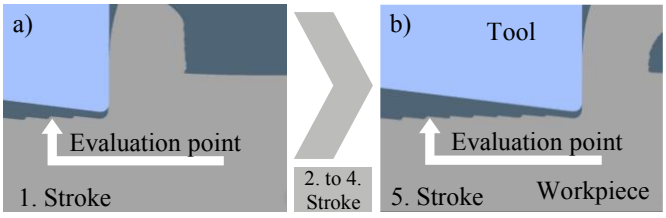

Figure 1: Position of the analysis a) after the first stroke b) after the fifth stroke

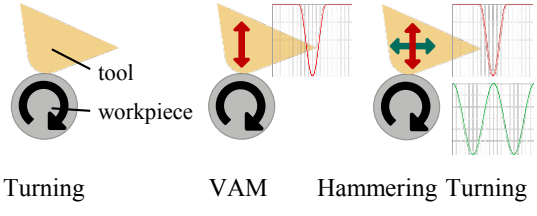

Figure 2: Kinematic scheme of the processes

2.3. Tool modelling

The tool is based on a regular CCMT-120408 insert which has an *83°* wedge angle. The rake angle is varied in three different configurations *-6°, 0°* and *6°*, which results in clearance angles, γ *=13°, 7°* and a very small one of *1°*. The cutting edge is seamlessly rounded with a cutting edge radius, r_β *= 20 µm*, while the depth of cut, a_p *= 0.1 mm*. The front part of the tool insert with a size of *0.5 mm x 0.5 mm* is modelled in the simulation. This section of the tool is fixed by a rigid tool holder, which also serves as a heat sink and moves the tool in the form of the kinematics for the turning process. The tool is modelled as a fully plastic deformable body with material properties of a solid-carbide grade K10 (*6%* mass fraction of cobalt), this has a high Young's modulus, *E = 630 GPa*, which leads to less displacement in the simulation. The tool is meshed using static mesh properties with a spatial discretization of *0.01 mm* in the whole domain, while in the area of tool to workpiece contact a refinement of *0.005 mm* is used.

2.4. Workpiece modelling / Material model

The workpiece is defined as a regular rectangle (*2 mm x 1 mm*) with corresponding connection faces to the workpiece holder. The material behavior of AISI 4140 q&t (temperature of *450 °C*) is modelled by a validated subroutine based on a Voce-constitutive strain hardening model with high temperature softening [8]. The formal structure of the model is given in equation 1. The flow stress σ depends on the plastic strain ε_{pl}, the strain rate $\dot{\varepsilon}_{pl}$ and the temperature *T* [9]. Where $g(T, T_{tr})$ is a softening term, ϵ_p is the plastic creep and $G(T)$ represents the shear modulus. The material specific parameters σ_0^*, n, m, σ_{G0}, σ_1, θ_1, and θ_0 were obtained experimentally and listet in Table 2 [10]. Due to excessive material deformation of the workpiece paired with huge gradients in space and time e.g. strain and strain-rate, resulting from the cutting process, as well as non-linear material behavior a fine discretization of the domain in time and space is crucial in order to sufficiently resolve the process. This is particularly crucial for the residual stresses, which exhibit large gradients in the very thin surface layer. Therefore a very fine mesh of element size and small timestep have to be set. The spatial discretization is also done with quad elements because of the higher number of degrees of freedom due to one more node per element compared to triangle meshes, and therefore a less stiff element behavior, which is more suitable for high deformations of the elements. The resolution is varying between *0.016 mm* for the

Table 2: Material Parameters

Material specific parameters	Value
σ_0^*	1329.84 MPa
n	0.74207
m	11.39618
σ_{G0}	1260 MPa
σ_1	150 MPa
θ_1	150 MPa
θ_0	10.5 MPa

$$\sigma = \underbrace{\sigma_0^* \cdot \left(1 - \left(\frac{T}{T_0}\right)^n\right)^m}_{\sigma^*} + \underbrace{\left(\sigma_{G0} + \left(\sigma_1 + \theta_1 \cdot \overline{\epsilon_p}\right) \cdot \left(1 - \exp\left(-\frac{\theta_1 \cdot \overline{\epsilon_p}}{\theta_0}\right)\right)\right)}_{\sigma_G} \cdot \frac{G(T)}{G(0K)} \cdot g(T, T_{tr}) \quad (1)$$

$$\sigma = \begin{cases} \sigma^* + \sigma_G & T < T_{crit} \text{ and } T < T_0 \\ \sigma_G & T_0 < T \leq T_{crit} \\ \sigma^* + \sigma_G \cdot g(T, T_{tr}) & T_{crit} < T \text{ and } T < T_0 \\ \sigma_G \cdot g(T, T_{tr}) & T_{crit} < T \text{ and } T_0 < T \end{cases}$$

majority of the domain and *0.001 mm* in the contact region where high gradients, e.g. strain, temperature and stresses, are to be expected. Because of the highly dynamic process the minimization of the resulting mesh distortion is crucial for obtaining a stable and high quality solution of the simulation. The meshing algorithm and the remeshing parameters are very important to get a fast converging solution in the solving procedure, therefore the remeshing with advancing front quad algorithm is chosen. The trigger values for remeshing in the simulation are set to 0.4 for the element strain and *0.001 mm* tool penetration. The number of elements increases from *28,000* to roughly *350,000* throughout the entire simulation.

2.5. Contact properties and boundary conditions

A widely used friction model of combined shear stress and coulomb friction approach is used, where the shear stress friction coefficient is set to *0.18* and the coulomb friction coefficient set to *0.3*. The contact between the holder and the respective bodies is glued, while the contact between the tool and the workpiece is represented by the friction model. The overall ambient temperature is set to *20°C*. The heat transfer coefficient for both the tool and the workpiece to environment is set to *20 W/m² K* while the heat transfer coefficient from tool to workpiece is calculated automatically from the material parameters.

3. Results and discussion

3.1. Influence of the rake angle on the residual stresses

The plastic deformation of the surface by the hammer strokes leads to residual compressive stresses in the subsurface workpiece layer. Figure 3 a) shows the residual stresses after VAM, as well as after only turning depending on the rake angle. For only turning maximum compressive residual stresses of *-165 MPa* are present for the negative rake angle. In addition, the depth of change in residual stresses is very small at about *75 µm*. The range and level of residual stresses caused by the VAM are significantly higher. Here, maximum residual compressive stresses of *-683 MPa* are simulated with a rake angle, γ *= 0°*. The distribution of the residual stresses exhibits similar characteristics regardless of the angle. Very significant is the different position of the maximum residual tensile stresses in a depth below the surface of *490 µm, 360 µm* and *290 µm*, which increases from negative to positive rake angle

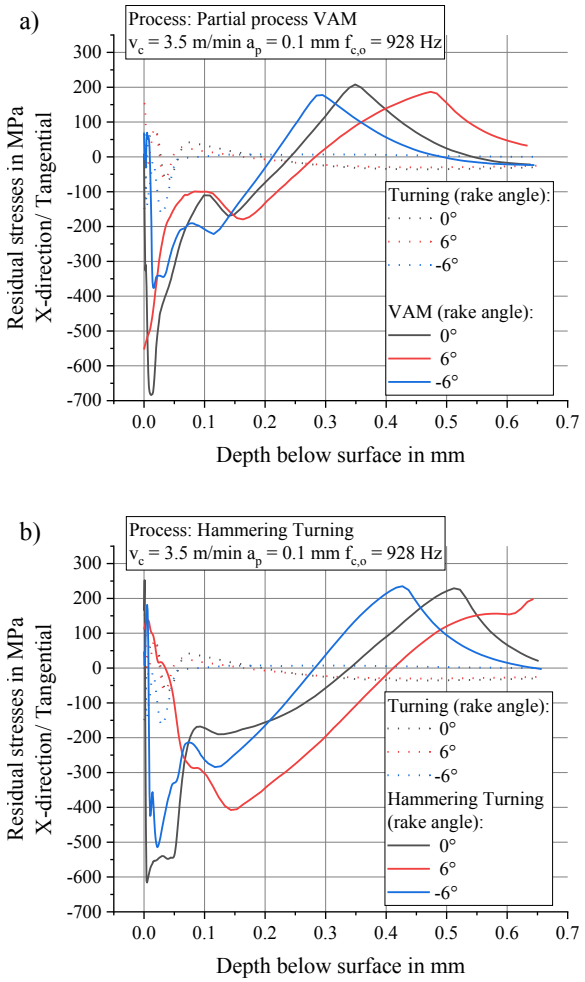

Figure 3: Residual stresses depending on the rake angle

of the tool. The magnitude of the maximum tensile stresses is nearly unaffected, while the maximum compressive residual stresses are significantly affected. Figure 3 b) shows the simulated residual stresses after Hammering Turning. The distribution of residual stresses is not as characteristic as for VAM. A shift of the position of the maximum tensile residual stresses to greater depths becomes clear, which is probably due to the fact that during the hammer stroke the tangential sliding component is reduced and thus more extensive plastic deformations can be introduced into the material and thus residual stresses. As the rake angle increases, the depth of the minima or maxima also increases. A rake angle of *6°* almost leads to a superposition of the two stress maxima. However, since the evaluation depth was only set to *650 µm*, this cannot be clearly identified. The minima, which are otherwise strictly defined in the VAM, are clearly stretched here and almost have a plateau-like character. The changed characteristics at a rake angl, $\gamma = 6°$ and a resulting very small clearance angle of *1°* leads to a large contact area between tool and workpiece, which is accompanied in the process by extensive material displacement and large forces. This can explain the large depth of the tensile residual stress maxima. The stresses after VAM and hammering turning show siginficantly higher and deeper compressive stresses than in the case with turning. This is due to the higher platic deformation of the surface layer caused by the hammer strokes.

3.2. Development of the stresses depending on the strokes

Since Hammering Turning is not a steady-state process, the development of stresses is also not continuous. The single hammer strokes cause a plastic deformation and a material flow that exceeds the actual effective area under the cutting edge. Figure 4 shows the development of the stresses occurring in the process for a tool orientation of rake angle, $\gamma = 0°$ over the five strokes and the stresses remaining after the cooling time and removal of the tool. A localized evaluation of the stress is given after one hammer stroke and the five following hammer strokes. A localised evaluation of the stresses after the strokes during the VAM and the combined process of Hammering Turning is carried out. For the VAM shown in Figure 4 a), a change in the stress distribution from the first to the second hammer stroke can be observed in the area near the surface, while no change in the distribution can be observed for the third to fifth strokes. This means that the area of influence of the plastically deformed zone extends up to two indentations. The distance between the indentation is $d_i = 63\ \mu m$. Considering the development of stresses in Hammering Turning in Figure 4 b), the influence of the plastically deformed zone is greater here. Therefore, a change in the stress distribution can be seen up to three hammer strokes, while the distribution after the fifth stroke is not detectably different from the third. This shows that by decoupling the cutting speed during Hammering Turning, a larger influenced zone can be achieved compared to VAM, where a tangential sliding component remains. The amplitude of the hammer stroke results here more completely in a material flow. In both the VAM and the Hammering Turning processes, a change in the stress distribution from the first to the second hammer stroke can be observed. In the very near surface layer down to a depth of *100 µm*, a completely different characteristic is observed. The local maxima and minima of the first stroke result in a deeper saddle point after the second stroke. This indicates a significant flow of material between these strokes, which is accompanied by a strong redistribution of stresses. Likewise, both processes show a significant relaxation of the stress after cooling and removal of the tool geometry in the simulation. Since the temperatures occurring at the low cutting speed are not particularly high, the stress relaxation caused by the removal of the tool geometry must be primarily accountable here. The two-dimensional FEM simulation makes it possible to investigate the redistribution of the stresses and the material flow during processing in a simplified process model. Figure 5 shows the stresses in the X-direction or cutting direction for a complete cycle of VAM a)-d) and Hammering Turning e)-h) in four states. Clearly visible in e) is the local compressive stress maximum after a hammer stroke directly below the cutting edge or the formed indentation. This is around 60 µm below the surface. These compressive stresses are reduced by the cutting and the effective forces in Figure 5 f). Here, it is explicitly not correct to speak of residual stresses, as this state is not in thermal and

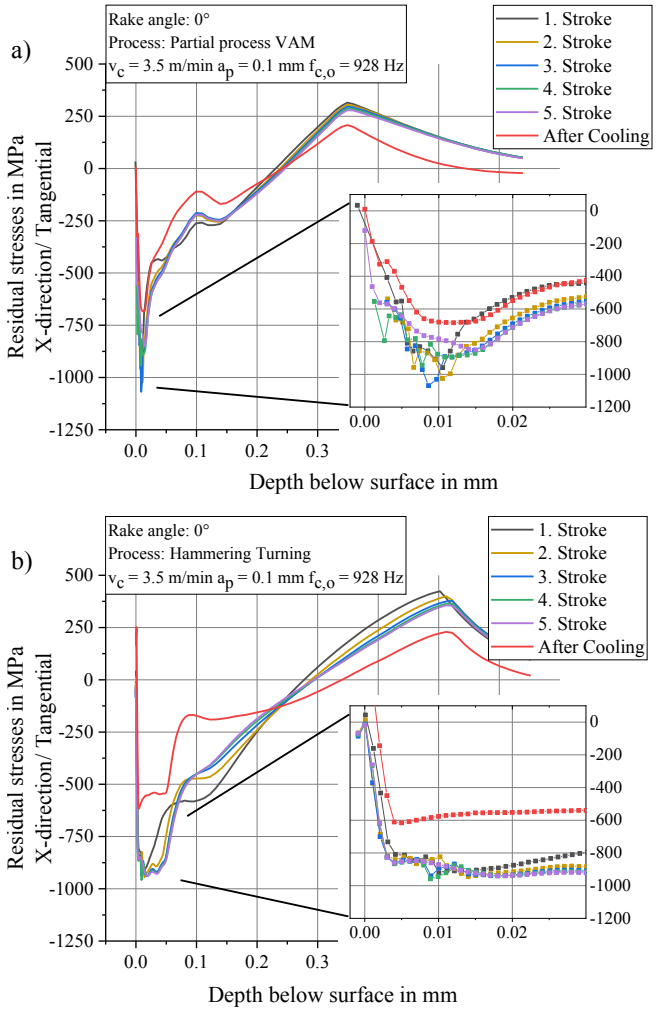

Figure 4: Stresses depending on the hammer strokes at rake angle, γ = 0°

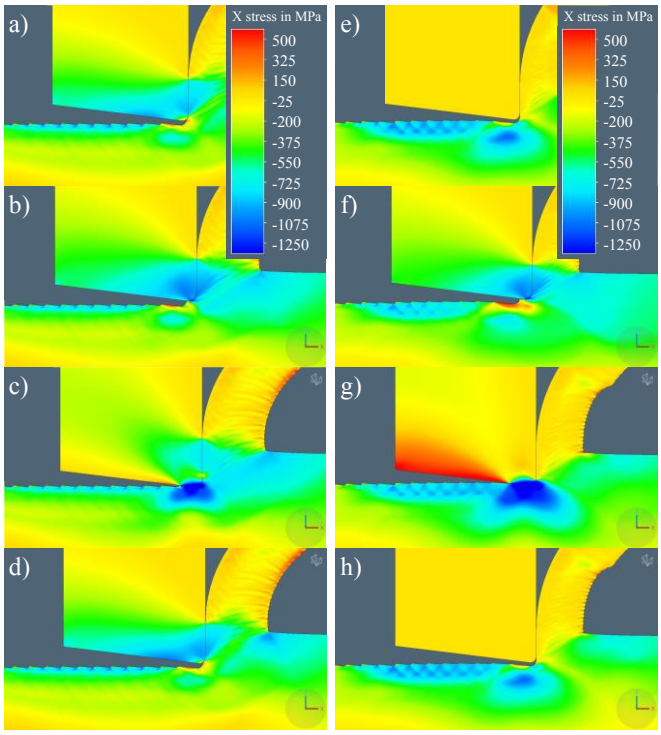

Figure 5: Distribution of stresses during one cycle of a hammer stroke at four points in time a)-d) VAM and e)-h) Hammering Turning

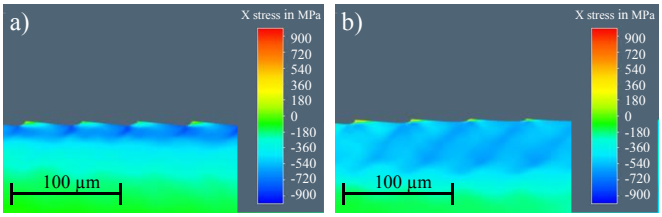

Figure 6: Residual stresses a) for VAM b) Hammering Turning

mechanical equilibrium without external forces. In Figure 5 g) the moment of the hammer stroke is shown. During a stroke, a cone of pressure builds up and a material flow that has moved in the opposite way to the cutting direction is encountered. This causes the layer directly under the surface to be compressed and the compressive stress maxima to be rearranged. This maxmimum moves with the tool path under the surface and leaves high compressive stresses under the surface. This also explains the strong change in the residual stress distribution from the first to the second stroke. Figure 5 a)-d) shows these four steps for the process of VAM, in which a decoupling from the cutting does not take place through a superimposed oscillation. Under the cutting edge in the surface layer, there is not such a pronounced compressive stress maximum. However, it should also be noted here that due to the lack of decoupling of the cutting, external forces are applied here which have an effect on the stresses. In step b) or f), comparable stress states are present in both processes, which is to be expected for the moment of cutting during Hammering Turning. During VAM, the compressive stresses are less pronounced. This also results, as clearly visible in step h), in a lower depth of the compressive stresses. Figure 6 shows the residual stresses after cooling for the two processes. It can be seen that for the VAM higher residual compressive stresses are localised at the surface, but for Hammering Turning these increase more deeply and reach almost twice the depth.

3.3. Material flow

In Figure 7, the material flow velocity in tangential direction is shown for VAM in a) and Hammering Turning in b) during a hammer stroke. Obviously visible is the backward material flow during Hammering Turning, which clearly reaches back two indentations of the previously machined surface. For the VAM, this material flow does not exist, as the tool continues to move in the cutting direction and this dominates the material flow. Thus, a larger plastic deformation is not possible during a hammer stroke. Likewise, different chip thicknesses can be observed at the same cutting depth. In Hammering Turning, the chip is much thinner and the shear angle steeper. This is possibly due to the higher effective cutting speed in Hammering Turning due to the superimposed vibration in the cutting direction or the high-frequency interrupted cut.

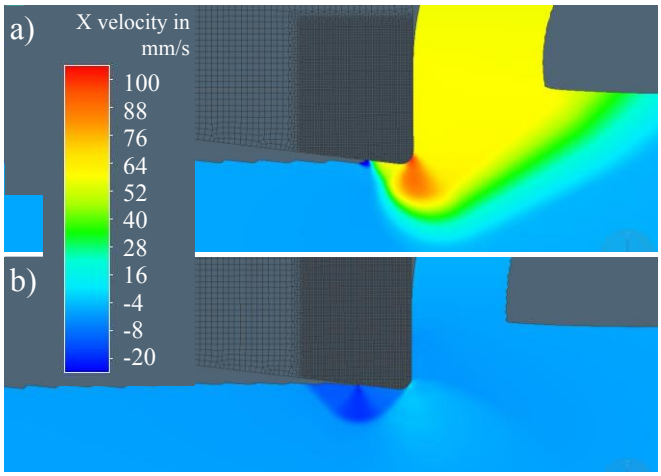

Figure 7: Materialflow for a hammer stroke a) VAM, b) Hammering Turning

3.4. Limitations and potential of the 2D approach

The modelling of Hammering Turning, which is a three-dimensional process of longitudinal turning, in a two-dimensional simulation represents a significant simplification of the process. The otherwise three-dimensional stress state and material flow can only be represented planarly two-dimensional, which is also in the real process only directly vertically under the cutting edge. The results of the simulation can therefore not provide quantitative values, but for the further development and scientific investigation of the novel process combination of Hammering Turning, a process understanding of the acting mechanisms can be achieved. The two-dimensional FEM simulation allows a fine spatial discretization with acceptable computation times.

4. Conclusion and outlook

In this work, the formation of residual stresses during Hammering Turning and turning with superimposed hammering (VAM) were compared. For the investigation, the complex three-dimensional process was simplified in a 2D FEM simulation in order to gain an understanding of the mechanism through this simplification. The following results about the Hammering Turning process have been obtained:

- The simulated residual compressive stresses in the surface layer during Hammering Turning and VAM are considerably larger than during turning.
- The simulations show that Hammering Turning can lead to deeper residual compressive stresses in the surface layer. This is a result of the lack of tangential velocity during a hammer stroke in Hammering Turning, which results in greater plastic deformation.
- The highest residual compressive stresses can be achieved directly beneath the surface of the component by a tool with a rake angle of *0°*. The maximum of the tensile residual stresses in the deeper surface layer is hardly influenced quantitativly, but with increasing rake angle the position is shifted further inwards.
- The formation of residual stresses is not continuous and still changes even when the tool has already left the machining zone with each hammer stroke. In Hammering Turning, the range of residual stress changes is greater. In the case of the VAM, there is an influence of up to three tool indentations; for the Hammering Turning, the influence of up to four tool indentations is verifiable.

After this qualitative investigation of the resulting stresses, these are to be investigated in the next step in a three-dimensional FEM simulation, which can be validated by residual stress measurements. The tribological properties of the surfaces hardened and microtextured by the Hammering Turning process will also be investigated. On the tool side, further investigations of the tool wear will be carried out to investigate the effects of the periodic cutting speed variation and tool load. Likewise, the changed chip formation observed in the simulations will be verified in experimental tests.

Acknowledgements

The authors thank the German Research Foundation for funding this study as part of the research project ZA 785/4-1.

References

[1] Bruzzone, A.A.G., Costa, H.L., Lonardo, P.M., Lucca, D.A., 2008. Advances in engineered surfaces for functional performance. CIRP Annals 57 (2), 750–769.
[2] Han, Z., Mu, Z., Yin, W., Li, W., Niu, S., Zhang, J., Ren, L., 2016. Biomimetic multifunctional surfaces inspired from animals. Advances in colloid and interface science 234, 27–50.
[3] Zheng, L., Chen, W., Huo, D., 2020. Review of vibration devices for vibration-assisted machining. Int J Adv Manuf Technol 108 (5-6), 1631–1651.
[4] Greco, A., Raphaelson, S., Ehmann, K., Wang, Q.J., Lin, C., 2009. Surface Texturing of Tribological Interfaces Using the Vibromechanical Texturing Method. Journal of Manufacturing Science and Engineering 131 (6), 430.
[5] Liu, X., Hu, X., Zhang, J., Wu, D., 2019. Study on the fabrication of micro-textured end face in one-dimensional ultrasonic vibration–assisted turning. Int J Adv Manuf Technol 105 (5-6), 2599–2613.
[6] Liu, X., Zhang, J., Li, L., 2021. Surface Integrity and Friction Performance of Brass H62 Textured by One-Dimensional Ultrasonic Vibration-Assisted Turning. Micromachines 12 (11).
[7] Schwalm, J., Mann, F., Gerstenmeyer, M., Zanger, F., Schulze, V., 2022. Main time-parallel mechanical surface treatment and surface texturing during machining. Procedia CIRP 108 (2), 240–245.
[8] Voce E., 1948. The relationship between stress and strain for homogeneous deformation. Journal of the Institute of Metals (74), 537–562.
[9] Authenrieth H., 2010. Numerische Analyse der Mikrozerspanung am Beispiel von normalisiertem C45E. Karlsruhe Institute of Technology, Dissertation.
[10] Segebade, E., Gerstenmeyer, M., Zanger, F., Schulze, V., 2017. Cutting Simulations Using a Commercially Available 2D/3D FEM Software for Forming. Procedia CIRP 58, 73–78.